Advances in Applied Mathematics and Mechanics
Adv. Appl. Math. Mech., Vol. **5**, No. 6, pp. 759-790

DOI: 10.4208/aamm.12-m1216
December 2013

Conservative and Finite Volume Methods for the Convection-Dominated Pricing Problem

Germán I. Ramírez-Espinoza[1,*] and Matthias Ehrhardt[2]

[1] *EON Global Commodities, Holzstraße 6, 40221 Düsseldorf, Germany*
[2] *Lehrstuhl für Angewandte Mathematik und Numerische Analysis, Fachbereich C – Mathematik und Naturwissenschaften, Bergische Universität Wuppertal, Gaußstr. 20, 42119 Wuppertal, Germany*

Received 9 March 2012; Accepted (in revised version) 10 October 2012

Available online 6 September 2013

Abstract. This work presents a comparison study of different numerical methods to solve Black-Scholes-type partial differential equations (PDE) in the convection-dominated case, i.e., for European options, if the ratio of the risk-free interest rate and the squared volatility-known in fluid dynamics as Péclet number-is high. For Asian options, additional similar problems arise when the "spatial" variable, the stock price, is close to zero.

Here we focus on three methods: the exponentially fitted scheme, a modification of Wang's finite volume method specially designed for the Black-Scholes equation, and the Kurganov-Tadmor scheme for a general convection-diffusion equation, that is applied for the first time to option pricing problems. Special emphasis is put in the Kurganov-Tadmor because its flexibility allows the simulation of a great variety of types of options and it exhibits quadratic convergence. For the reduction technique proposed by Wilmott, a put-call parity is presented based on the similarity reduction and the put-call parity expression for Asian options. Finally, we present experiments and comparisons with different (non)linear Black-Scholes PDEs.

AMS subject classifications: 65M10, 91B25

Key words: Black-Scholes equation, convection-dominated case, exponential fitting methods, fitted finite volume method, Kurganov-Tadmor scheme, minmod limiter.

1 Introduction

An option is an instrument in which two parties agree to the possibility to exchange an asset, the underlying, at a predefined price and maturity. The payoff represents the

*Corresponding author.
Email: german.rmz@gmail.com (G. Ramírez-Espinoza), ehrhardt@math.uni-wuppertal.de (M. Ehrhardt)

profit-loss profile defined by the option for a given range of prices. There exist a great variety of options ranging from European options, to American, Asian, Barrier options, Binary options, etc., and many of these derivatives are valuated with the classical pricing formulae developed by Black, Scholes and Merton. The type of the option refers in many cases to the type of payoff profile of the option but for the European and American option, the type refers to its maturity: the maturity of a European option is fixed whereas the American option can be exercised at any time before the maturity, e.g., there exist Asian options of European and American type.

The partial differential equation (PDE) proposed by Black, Scholes and Merton is known as the Black-Scholes equation and is a special case of a more general convection-diffusion equation that also arises in other areas like fluid dynamics. Due to its convective term, the solution is a traveling wave transporting the initial data and due to the diffusive term the data is dissipated: a dissipating traveling wave. If the diffusion coefficient is small compared to to the transport coefficient then the solution behaves mainly like a traveling wave and the equation is said to be convection-dominated. For purely first order hyperbolic PDEs, it is known [9] that standard methods fail to obtain an acceptable approximation when discontinuities are present in the initial data and a similar issue is observed in the convection-diffusion equation in the convection-dominated case and discontinuous initial data. Some schemes like the Lax-Friedrichs or the upwind method were proposed to obtain satisfactory approximations for hyperbolic PDEs, but artificial diffusion is introduced by the method which leads to smeared solutions. In terms of the Black-Scholes equation, this behavior appears if the squared volatility is small in comparison with the risk-free rate.

When solving numerically the Black-Scholes PDE it is useful to reverse transform the time variable to use the payoff function (terminal condition) as the initial condition (IC) of the system. Albeit the payoff of an European option is non-smooth and the numerical solution for the price is acceptable, artificial oscillations appear near the strike price when the first numerical derivative with respect to the underlying price of this approximation is obtained. These oscillations are worst when higher derivatives are calculated. Having access to the first derivative of the option price is important to measure the sensitivity of the option to movements on the price of the underlying or other parameters like volatility. Higher derivatives of the option price also provide important information about the behavior of the option. These quantities are known in the financial literature as the *Greeks*. Due to the Greeks being relevant for the quantitative analysts, reliable numerical methods are required for the pricing of options which not only provide a good approximation for the price, but also for its derivatives.

In this paper finite difference methods (FDMs) for the Black-Scholes equation with a wide range of parameters, including the critical convection-dominated case are considered. Conservative methods, a special family of FDMs and also denoted as finite volume methods (FVMs), are presented as the method of choice to solve convection-dominated problems. Two conservative methods are studied: the Kurganov-Tadmor scheme [14], a high resolution method for a general convection-diffusion equation which exhibits

quadratic convergence and introduces small artificial viscosity in comparison to other methods, e.g., the Lax-Friedrichs scheme, and the Wang scheme [18] for an European option in which the flux of the Black-Scholes equation in conservative form is solved analytically and exhibits linear convergence. We also consider the exponentially fitted scheme proposed by Il'in [12] (see also [16]) and then presented in the context of finance by Duffy [5]. According to the authors' knowledge, this is the first time the Kurganov-Tadmor scheme is applied to option pricing problems.

2 Options and pricing equations

2.1 Option pricing

An option is a financial instrument in which two parties agree to exchange an asset at a predefined price or *strike* K and date or *maturity* T. By paying an up-front quantity-known as the price or *premium* of the option-the holder of the contract has the right, but not the obligation, to buy/sell the asset at maturity. The underlying asset on the contract is typically a stock or a commodity but the possibilities are immense; for instance, it is possible to create an option with a *future* or a *swap* as the underlying-the latter is called *swaption* in the financial literature. An option in which the holder has the right to buy the underlying is a call option whereas if the contract gives the holder the right to sell the underlying then it is denominated as a put option.

The value of a call option from the perspective of the holder at maturity time is shown in Fig. 1(a). The price of the option is denoted as P and the strike price as K. The x-axis represents the price of the underlying asset whereas the red line represents the value of the option. If the price of the underlying is less than the strike price, the option is worthless for the holder because it is possible to buy the underlying at a lower price. When the price of the underlying is greater than $K+P$ then the value of the option increases and the holder of the option profits from the difference s_T-P-K where s_T is the price of the underlying at maturity. In Fig. 1(b) the payoff of a put option is shown and in this case the holder profits from the difference $K-s_T-P$.

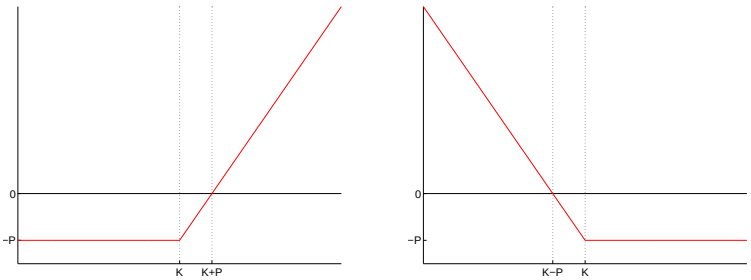

(a) Call option. (b) Put option.

Figure 1: Payoffs of a *long* position on an option with strike price K and premium P.

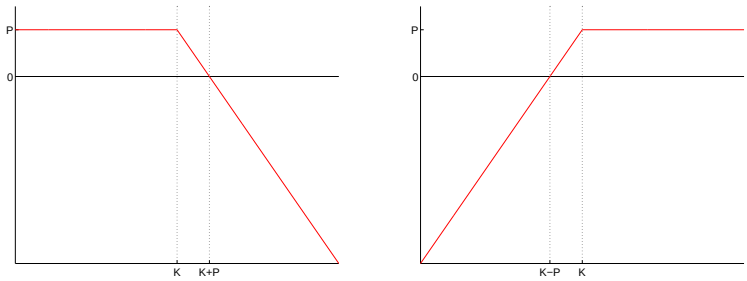

(a) Call option. (b) Put option.

Figure 2: Payoffs of a *short* position on an option with strike price K and premium P.

Both payoffs in Fig. 1 are referred as *long* positions on an option. In financial terminology, *going long* on a financial instrument is used as a synonym of buying it and therefore benefiting when the price increases.

In contrast to the long positions, *short* positions on a financial instrument is synonym of selling it. The payoff for a short position on an option is shown in Fig. 2. What we have described up to now as an option is known in the financial literature as *European* option. Another important type of option is known as *American* option which can be exercised at any time before the maturity, but the payoff is the same as in the case for the European type. A third type are the Asian options that define a payoff depending on the temporal average of the price of the underlying.

For the same maturity, strike price and underlying, a relation between the price of a call and a put option under a frictionless market can be defined. This relationship is known as the *put-call parity* and arises from the fact that with combinations of long/short calls and long/short puts it is possible to create *synthetic* instruments with the same payoff as the real ones. For instance, by combining a long call and a short put on a stock, it is possible to create an instrument with the same payoff as the underlying, i.e., a synthetic stock; it is also possible to create a synthetic long call by creating a portfolio of a long put and holding a stock. A relation between a call and a put in terms of the price of the stock must be fulfilled to keep an arbitrage-free market.

For a European option with maturity T and strike K and ignoring the premium of the option, we can create two portfolios to obtain the desired relationship. In the first portfolio a long call and a short put is held with payoff $s-K$. The second portfolio holds a long stock and K bonds with maturity T that pays a unit of currency at T, achieving a payoff $s-K$. By arbitrage arguments, these portfolios have the same price

$$v_C(s,t)-v_P(s,t)=s_t-Kb(t,T), \tag{2.1}$$

where $b(t,T)$ is the bond price with maturity T, $v(s,t)$ the option price and s_t the stock price at t. A constant risk-free interest rate-required by the Black-Scholes model-defines the price of the bond as $b(t,T)=\exp(-r(T-t))$, which completes (2.1).

Besides the obvious theoretical and practical importance of the put-call parity, it is

also useful in numerical analysis to obtain boundary conditions for pricing schemes: when the boundary conditions (BCs) are known only for a put or call, the unknown BCs for the other instrument can be easily obtained with Eq. (2.1).

The Black-Scholes equation for option pricing is a backward-in-time parabolic PDE:

$$\frac{\partial v(s,t)}{\partial t}+\frac{1}{2}\sigma^2 s^2\frac{\partial^2 v(s,t)}{\partial s^2}+rs\frac{\partial v(s,t)}{\partial s}-rv(s,t)=0,\quad s>0,\quad t\in[0,T], \tag{2.2}$$

where r denotes the continuously compounded, annualized risk-free interest rate, σ is the volatility of the stock price s, K is the strike price and T is the maturity.

For a call option, the boundary conditions can be expressed as

$$\begin{aligned} &v(0,t)=0,\\ &v(s,t)\to s\exp(-d(T-t))-K\exp(-r(T-t)) \quad \text{for } s\to\infty \end{aligned}$$

and the terminal condition is defined as

$$v(s,T)=(s-K)^+,\qquad (a)^+:=\max(a,0). \tag{2.3}$$

Contrary, for a put option the boundary conditions are

$$\begin{aligned} &v(s,t)=K\exp(-r(T-t))-s\exp(-d(T-t)) \quad \text{for } s\to 0,\\ &v(s,t)=0 \quad \text{for } s\to\infty, \end{aligned}$$

and the terminal condition reads $v(s,T)=(K-s)^+$.

2.2 Asian options

An Asian option is a path-dependent option and the payoff is determined by the average of the price of the underlying instrument. The price of an Asian option is denoted by $v(s,a,t)$ where $a(t)$ is the continuous arithmetic average of s over the interval $[0,t]$

$$a(t):=\frac{1}{t}\int_0^t s(\tau)d\tau.$$

The inclusion of the average $a(t)$ leads to a new "spatial" dimension in (2.2), cf. [17]

$$\frac{\partial v}{\partial t}+\frac{1}{2}\sigma^2 s^2\frac{\partial^2 v}{\partial s^2}+rs\frac{\partial v}{\partial s}-rv+\frac{1}{t}(s-a)\frac{\partial v}{\partial a}=0 \tag{2.4}$$

with the following payoff or terminal condition:

$$\text{for a call}\quad \begin{cases}(a-K)^+ & \text{fixed strike,}\\ (s-a)^+ & \text{floating strike,}\end{cases}\qquad \text{for a put}\quad \begin{cases}(K-a)^+ & \text{fixed strike,}\\ (a-s)^+ & \text{floating strike.}\end{cases}$$

Eq. (2.4) is supplied with the boundary condition at $s=0$

$$\frac{\partial v}{\partial t}-\frac{a}{t}\frac{\partial v}{\partial a}-rv=0,$$

whereas for $s\to\infty$ we have

$$\frac{\partial v}{\partial t}+\frac{1}{t}(s-a)\frac{\partial v}{\partial a}=0.$$

In (2.4) there are no diffusion terms with respect to $a(t)$, i.e., a purely transport behavior is expected in that direction. Moreover, the put-call parity for an Asian option reads

$$v_C-v_P=s-\frac{s}{rT}\left[1-\exp(-r(T-t))\right]-\exp(-r(T-t))\frac{1}{T}\int_0^t s(\tau)d\tau. \tag{2.5}$$

2.3 The Wilmott similarity reduction

It is possible to reduce the full PDE for Asian options (2.4) to one spatial and one temporal dimension by using a similarity reduction proposed by Wilmott [19].

Let us consider the floating strike payoff of a call option

$$(s-a)^+=s\left(1-\frac{1}{st}\int_0^t s(\tau)d\tau\right)$$

and by letting

$$x=\frac{1}{s}\int_0^t s(\tau)d\tau, \tag{2.6}$$

we substitute the separation ansatz $v(s,a,t)=s\cdot y(x,t)$ into (2.4) to obtain

$$\frac{\partial y}{\partial t}+\frac{\sigma^2}{2}x^2\frac{\partial^2 y}{\partial x^2}+(1-rx)\frac{\partial y}{\partial x}=0 \tag{2.7}$$

with the terminal condition

$$y(x,T)=\left(1-\frac{1}{T}x\right)^+. \tag{2.8}$$

The boundary conditions for a call are easily obtained by taking the limits of (2.7), e.g., for $x\to 0$, the Eq. (2.7) is

$$\frac{\partial y}{\partial t}+\frac{\partial y}{\partial x}=0, \tag{2.9}$$

because, assuming $y(x,t)$ is bounded, it is possible to show that the term

$$x^2\frac{\partial^2 y}{\partial x^2}\to 0 \quad \text{for } x\to 0,$$

cf. [17], whereas for the case $x\to\infty$ it can be seen from the payoff (2.8) that the option is not exercised, therefore $y=0$.

This PDE (2.7) for Asian options is advantageous, computationally speaking, because only one spatial and one temporal dimension occurs, in contrast to the full PDE (2.4) which requires two spatial and one temporal dimension, leading to considerably higher computational costs and higher memory requirements.

With the separation ansatz $v(s,a,t)=sy(x,t)$, we write the put-call parity (2.5) as

$$\begin{aligned} y_C-y_P &=1-\frac{1}{rT}\big[1-\exp(-r(T-t))\big]f-\exp(-r(T-t))\frac{1}{sT}\int_0^t s(\tau)d\tau \\ &=1-\frac{1}{rT}\big[1-\exp(-r(T-t))\big]-\exp(-r(T-t))\frac{x}{T}, \end{aligned}$$

where the definition of the new independent variable (2.6) was used in the last row.

The boundary conditions for a put option are now readily available from the put-call parity equation.

Let us note that a drawback of the reduction is that it is only possible reduce the PDE in the case of a floating strike option.

2.4 The Rogers-Shi reduction

An alternative PDE was presented in [15] using a new variable:

$$x=\frac{1}{s}\Big[K-\int_0^t s(\tau)\mu(d\tau)\Big]$$

with μ as probability measure with density $\rho(t)$ such that

$$\rho(t)=\begin{cases}\dfrac{1}{T}, & \text{for a fixed strike option,}\\[2mm] \dfrac{1}{T}-\delta(T-\tau), & \text{for a floating strike option,}\end{cases}$$

where in the case for a floating strike option K is set to zero. This yields the PDE

$$\frac{\partial w}{\partial t}+\frac{\sigma^2}{2}x^2\frac{\partial^2 w}{\partial x^2}-(\rho(t)+rx)\frac{\partial w}{\partial x}=0$$

with the following terminal condition for a fixed strike call option

$$w(x,T)=\min(0,x)=:(x)^- \tag{2.10}$$

and for a floating strike put option

$$w(x,T)=(1+x)^-. \tag{2.11}$$

Boundary conditions (BCs) are defined depending on the type of payoff. For a fixed strike call we have

$$w(x,t)=\frac{\exp(r(T-t))-1}{r}-x \quad \text{for } x<0$$

and from the payoff (2.10) we obtain the boundary condition

$$w(x,t)=0 \quad \text{for } x\to\infty.$$

On the other hand, for a floating strike put we obtain

$$w(x,t)=\frac{\exp(r(T-t))-1}{rT}-\exp(r(T-t))-x \quad \text{for } x\ll 0$$

and from the corresponding payoff (2.11) we obtain the other boundary condition

$$w(x,t)=0 \quad \text{for } x>-1.$$

The price of the option is then $s_0 w(K/s_0,0)$ for the case of a fixed strike option and $s_0 w(0,0)$ for the case of a floating strike, where s_0 is the current price of the underlying.

3 Finite difference methods

For the case of the Black-Scholes equations-or generally speaking, the convection-diffusion equation-it is well known [5, 9, 17] that standard finite difference methods (FDMs) often does not yield satisfactory results yielding unphysical oscillations. Hence, there is the need for specially designed FDMs; we focus on: the exponentially fitted method, Wang's finite volume method, and the Kugranov-Tadmor scheme.

Let us recall that the option price is a function of the stock price s and time t and is denoted by $v(s,t)$. Its pointwise approximation is $V_i^n := v(s_i,t_n)+\epsilon$, where ϵ is the truncation error.

For convenience, a time reversal $t^*=t-T$ is performed. Doing so, the IC of the system is the payoff of the option and (2.2) is then transformed to

$$\frac{\partial v(s,t^*)}{\partial t^*}=\frac{\sigma^2}{2}s^2\frac{\partial^2 v(s,t^*)}{\partial s^2}+(r-d)s\frac{\partial v(s,t^*)}{\partial s}-rv(s,t^*), \tag{3.1}$$

where we included the continuous dividend yield d. In the sequel this star notation is dropped for simplicity and the forward time is again written as t. A "spatial" mesh for the stock price $s\in[s_{\min},s_{\max}]$ is defined with $N+2$ points s_i for $i=0,1,\cdots,N+1$,

$$s_{\min}=s_0<s_1<\cdots<s_N<s_{N+1}=s_{\max},$$

with $\Delta s=(s_{\max}-s_{\min})/(N+1)$. The time $t\in[T,0]$ is discretized in M points t_j

$$T=t_1>t_2>\cdots>t_M=0 \quad \text{with } \Delta t=T/(M-1).$$

For the case of Dirichlet BCs, we define $v(s_{\min},t)=g_1(t)$, $v(s_{\max},t)=g_2(t)$.

3.1 Exponentially fitted schemes

Standard FDMs may lead to unstable (or at least unphysical oscillatory) solutions for convection-diffusion type equations, especially in the case of large Péclet numbers. Here a technique proposed by Il'in [12] which was later applied to the pricing problem with the Black-Scholes equation by Duffy [5] is presented. This implicit *exponential fitted method (EFM)* for the Black-Scholes equation is

$$\frac{V_i^{n+1}-V_i^n}{\Delta t}=\rho\frac{\sigma^2}{2}s_i^2\frac{V_{i+1}^{n+1}-2V_i^{n+1}+V_{i-1}^{n+1}}{\Delta s^2}+(r-d)s_i\frac{V_{i+1}^{n+1}-V_{i-1}^{n+1}}{2\Delta s}-rV_i^{n+1},$$
$$\rho=\frac{1}{2}\zeta\coth\left(\frac{1}{2}\zeta\right)\quad\text{and}\quad\zeta=\frac{(r-d)s_i\Delta s}{\frac{1}{2}\sigma^2s_i^2}=\frac{2(r-d)\Delta s}{\sigma^2 s_i}.$$

By rearranging the terms, the scheme can be rewritten as

$$\alpha_i V_{i-1}^{n+1}+\beta_i V_i^{n+1}+\gamma_i V_{i+1}^{n+1}=V_i^n \tag{3.2}$$

with

$$\alpha_i=-\frac{1}{2}\left(\rho\frac{\sigma^2s_i^2\Delta t}{\Delta s^2}-\frac{(r-d)s_i\Delta t}{\Delta s}\right),\qquad\beta_i=1+r\Delta t+\rho\frac{\sigma^2s_i^2\Delta t}{\Delta s^2},$$
$$\gamma_i=-\frac{1}{2}\left(\rho\frac{\sigma^2s_i^2\Delta t}{\Delta s^2}+\frac{(r-d)s_i\Delta t}{\Delta s}\right)\quad\text{for } i=1,2\cdots,N\quad\text{and}\quad n=1,2,\cdots M.$$

Furthermore, the scheme (3.2) can be rewritten in the compact matrix form

$$\begin{bmatrix}\beta_1&\gamma_1&&&\\ \alpha_2&\beta_2&\gamma_2&&\\ &\ddots&\ddots&\ddots&\\ &&\alpha_{N-1}&\beta_{N-1}&\gamma_{N-1}\\ &&&\alpha_N&\beta_N\end{bmatrix}\begin{bmatrix}V_1^{n+1}\\ V_2^{n+1}\\ \vdots\\ V_{N-1}^{n+1}\\ V_N^{n+1}\end{bmatrix}=\begin{bmatrix}V_1^n-\alpha_1V_0^n\\ V_2^n\\ \vdots\\ V_{N-1}^n\\ V_N^n-\gamma_NV_{N+1}^n\end{bmatrix} \tag{3.3}$$

with boundary conditions included. The unknown vector V^{n+1} is obtained by solving a tridiagonal system of equations with computational effort $\mathcal{O}(N)$ at each time step.

The simulation results for the derivative price with $r=0.05$, $d=0$, $\sigma=0.01$, $K=13$, $T=1$, $s_{\min}=10$, $s_{\max}=15$, $N=50$ and $M=100$ is shown in Fig. 3(a). The numerical derivative of the option's price with respect to the stock price is shown in Fig. 3(b). Spurious oscillations are not visible. On the other hand, the artificial diffusion introduced by the method is evident now. Table 1 shows the error for different discretization grids. It is evident that the computational order of convergence of the EFM is in line with the theoretical order of convergence $\mathcal{O}(\Delta s)$ obtained in [12].

Table 1: Error of the price for the EFM for different step sizes.

$N\times M$	20×200	40×200	60×200	80×200	100×200
$\|v(s_i,T)-V_i^M\|_\infty$	0.10371	0.06014	0.04111	0.03051	0.02318
Δs	0.23810	0.12195	0.08197	0.06173	0.04950

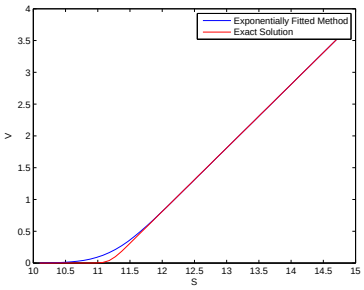

(a) Comparison between exact and numerical solution of a plain-vanilla European call with EFM.

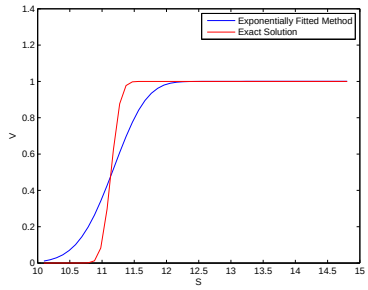

(b) No spurious oscillation observed, solution is smoothed out by EFM.

Figure 3: Exponential Fitting Method applied to the Black-Scholes equation.

4 Wang's fitted finite volume method

Finite Volume Methods (FVMs) are derived on the basis of the integral formulation of a conservation law mimicking underlying conservation principles of the PDE. The FVM defines a volume surrounding each discretization point, called cells, and inside these cells, an approximation to the average value of the unknown is determined. Let us consider the discretization of the general conservation law in 1D

$$\frac{\partial}{\partial t}u(x,t)+\frac{\partial}{\partial x}f(u(x,t))=0, \tag{4.1}$$

where $x\in[a,b]$ and f denotes the flux of the system.

We start by defining an admissible mesh suitable for FVMs on an interval $x\in[a,b]$. A family of equidistant points as $(x_i)_{i=0,\cdots,N+1}$ and a family of midpoints $(I_i)_{i=1,\cdots,N}$ such that $I_i=[x_{i-1/2},x_{i+1/2}]$ is defined resulting in a grid

$$x_0=x_{\frac{1}{2}}=a<x_1<x_{\frac{3}{4}}<\cdots<x_{i-\frac{1}{2}}<x_i<x_{i+\frac{1}{2}}<x_N<x_{N+\frac{1}{2}}=x_{N+1}=b \tag{4.2}$$

with $x_{i\pm1/2}:=x_i\pm\Delta x/2$, cf. [8]. Integrating (4.1) on the rectangle $I_i\times[t,t+\Delta t]$ we have

$$\int_{I_i}u(x,t+\Delta t)dx-\int_{I_i}u(x,t)dx=-\int_t^{t+\Delta t}f(u(x_{i+\frac{1}{2}},t))dt+\int_t^{t+\Delta t}f(u(x_{i-\frac{1}{2}},t))dt$$

and with $\bar{U}_i^n$ as the cell average value of $u(x,t)$ in the interval I_i at time t_n we have

$$\bar{U}_i^{n+1}=\bar{U}_i^n-\frac{1}{\Delta x}\Big[\int_t^{t+\Delta t}f(u(x_{i+\frac{1}{2}},t))dt-\int_t^{t+\Delta t}f(u(x_{i-\frac{1}{2}},t))dt\Big]. \tag{4.3}$$

The integral of the flux with respect to time is approximated by the *numerical flux*

$$F_{i+\frac{1}{2}}^n\approx\frac{1}{\Delta t}\int_t^{t+\Delta t}f(u(x_{i+\frac{1}{2}},t))dt$$

and we can now express the fully discrete version of (4.3) as the conservative FDM

$$\bar{U}_i^{n+1} = \bar{U}_i^n - \frac{\Delta t}{\Delta x}\left[F^n_{i+\frac{1}{2}} - F^n_{i-\frac{1}{2}}\right].$$

Wang presented in [18] a fitted FVM for the Black-Scholes equation with non-constant coefficients. This section briefly reviews the essential parts of the derivation. For transforming equation (2.2) to a problem with homogeneous Dirichlet boundary conditions, the function $f(S,t) = -\mathcal{L}V_0$ is introduced in both sides of (2.2) where

$$V_0 = g_1(t) + \frac{1}{s_T}\left[g_1(t) - g_2(t)\right]s$$

and $\mathcal{L}$ is the differential operator in (2.2).

By defining the variable $u = V - V_0$, it is possible to rewrite the Black-Scholes PDE in the self-adjoint form:

$$\frac{\partial u}{\partial t} - \frac{\partial}{\partial s}\left[a(t)s^2\frac{\partial u}{\partial s} + b(s,t)su\right] + c(s,t)u = f(s,t) \tag{4.4}$$

with

$$a(t) = \frac{1}{2}\sigma^2(t), \qquad b(s,t) = r(t) - \sigma^2(t), \qquad c(s,t) = r(t) - b(s,t).$$

An admissible mesh analogous to (4.2) is defined for the interval $s \in [0, s_{\max}]$ with $N+2$ grid points, given by a family $I_i = (s_{i-1/2}, s_{i+1/2})$ and a family $(s_i)_{i=0,\cdots,N+1}$

$$s_0 = s_{\frac{1}{2}} = 0 < s_1 < s_{\frac{3}{4}} < \cdots < s_{i-\frac{1}{2}} < s_i < s_{i+\frac{1}{2}} < \cdots < s_N < s_{N+\frac{1}{2}} = s_{N+1} = s_{\max} \tag{4.5}$$

with the "spatial" step size $\Delta s_i = s_{i+1} - s_i$ and $\Delta s = \max_{\forall i}(\Delta s_i)$. Integrating the Black-Scholes PDE in conservative form (4.4) over the cell $I_i = (s_{i-1/2}, s_{i+1/2})$ leads to

$$\int_{I_i}\frac{\partial u}{\partial t}ds - \left[s\left(as\frac{\partial u}{\partial s} + bu\right)\right]_{s_{i-\frac{1}{2}}}^{s_{i+\frac{1}{2}}} + \int_{I_i} cu ds = \int_{I_i} f ds. \tag{4.6}$$

By approximating the integrals in (4.6) with the midpoint rule we get

$$\frac{\partial U_i}{\partial t}\ell_i - \left[s_{i+\frac{1}{2}}\rho(u(s_{i+\frac{1}{2}},t)) - s_{i-\frac{1}{2}}\rho(u(s_{i-\frac{1}{2}},t))\right] + c_i U_i \ell_i = f_i \ell_i \tag{4.7}$$

with $\ell_i := s_{i+1/2} - s_{i-1/2}$, the discrete unknown is denoted by $U_i := u(s_i,t)$ and $c_i := c(s_i,t)$ and $f_i := f(s_i,t)$ for $i = 1,\cdots,N$. Thus, the flux $\rho(u(s,t))$ is defined as

$$\rho(u(s,t)) := a(t)s\frac{\partial u(s,t)}{\partial s} + b(s,t)u(s,t). \tag{4.8}$$

Due to the degeneracy of $\rho(u(s,t))$ at $s=0$, the flux must be treated separately both for the degenerate and non-degenerate case, cf. [18] for details. By inserting the expression for the numerical flux (4.8) in (4.7), we get the semi-discrete scheme

$$\frac{\partial U_i(t)}{\partial t}+\frac{1}{\ell_i}\left[e_{i,i-1}u_{i-1}(t)+e_{i,i}u_i(t)+e_{i,i+1}u_{i+1}(t)\right]=f_i, \tag{4.9}$$

where

$$e_{1,1}=\frac{s_1}{4}(a+b_{1+\frac{1}{2}})+\frac{b_{1+\frac{1}{2}}\cdot s_{1+\frac{1}{2}}\cdot s_1^{\alpha_1}}{s_2^{\alpha_1}-s_1^{\alpha_1}}+c_1\ell_1, \quad e_{1,2}=-\frac{b_{1+\frac{1}{2}}\cdot s_{1+\frac{1}{2}}\cdot s_2^{\alpha_1}}{s_2^{\alpha_1}-s_1^{\alpha_1}} \tag{4.10}$$

and

$$e_{i,i-1}=-\frac{b_{i-\frac{1}{2}}\cdot s_{i-\frac{1}{2}}\cdot s_{i-1}^{\alpha_{i-1}}}{s_i^{\alpha_{i-1}}-s_{i-1}^{\alpha_{i-1}}}, \qquad e_{i,i+1}=-\frac{b_{i+\frac{1}{2}}\cdot s_{i+\frac{1}{2}}\cdot s_{i+1}^{\alpha_i}}{s_{i+1}^{\alpha_i}-s_i^{\alpha_i}}, \tag{4.11a}$$

$$e_{i,i}=\frac{b_{i-\frac{1}{2}}\cdot s_{i-\frac{1}{2}}\cdot s_i^{\alpha_{i-1}}}{s_i^{\alpha_{i-1}}-s_{i-1}^{\alpha_{i-1}}}+\frac{b_{i+\frac{1}{2}}\cdot s_{i+\frac{1}{2}}\cdot s_i^{\alpha_i}}{s_{i+1}^{\alpha_i}-s_i^{\alpha_i}}+c_i\ell_i, \tag{4.11b}$$

expressions which, although it is not explicitly stated, depend on time because $a(t)$, $b(s,t)$ and $c(s,t)$. These $e_{i,i}$ form the following tridiagonal matrix $E\in\mathbb{R}^{N\times N}$

$$E=\begin{bmatrix} e_{1,1} & e_{1,2} & & & & & & \\ e_{2,1} & e_{2,2} & e_{2,3} & & & & & \\ & \ddots & \ddots & \ddots & & & & \\ & & e_{i,i-1} & e_{i,i} & e_{i,i+1} & & & \\ & & & \ddots & \ddots & \ddots & & \\ & & & & e_{N-1,N-2} & e_{N-1,N-1} & e_{N-1,N} \\ & & & & & e_{N,N-1} & e_{N,N} \end{bmatrix} \tag{4.12}$$

with $U(t)=(U_1(t),\cdots,U_N(t))^\top$, $F(t)=(f_1(t),\cdots,f_N(t))^\top$, (4.9) can be written as

$$\frac{\partial U(t)}{\partial t}+\Phi E(t)U(t)=F(t), \tag{4.13}$$

where $\Phi=\mathrm{diag}(1/\ell_1,1/\ell_2,\cdots,1/\ell_N)$. Redefining the coefficients (4.10) and (4.11) as

$$e_{1,1}=\frac{1}{\ell_1}\frac{s_1}{4}(a+b_{1+\frac{1}{2}})+\frac{1}{\ell_1}\frac{b_{1+\frac{1}{2}}\cdot s_{1+\frac{1}{2}}\cdot s_1^{\alpha_1}}{s_2^{\alpha_1}-s_1^{\alpha_1}}+c_1,$$
$$e_{i,i}=\frac{1}{\ell_i}\frac{b_{i-\frac{1}{2}}\cdot s_{i-\frac{1}{2}}\cdot s_i^{\alpha_{i-1}}}{s_i^{\alpha_{i-1}}-s_{i-1}^{\alpha_{i-1}}}+\frac{1}{\ell_i}\frac{b_{i+\frac{1}{2}}\cdot s_{i+\frac{1}{2}}\cdot s_i^{\alpha_i}}{s_{i+1}^{\alpha_i}-s_i^{\alpha_i}}+c_i,$$

it is possible to avoid a matrix-matrix multiplication (4.13), yielding

$$\frac{\partial U(t)}{\partial t}+\mathcal{E}(t)U(t)=F(t). \tag{4.14}$$

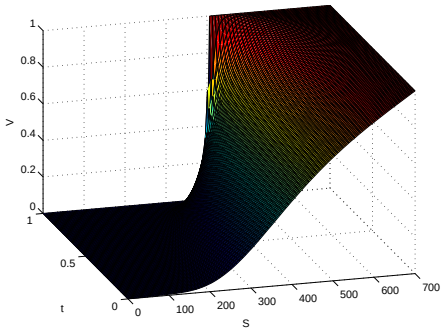

Figure 4: Cash-or-Nothing option price obtained with Wang's FV scheme.

Recall that Eqs. (4.13), (4.14) are first-order linear stiff ODE systems for $U_i(t)$.

We reproduced the results of Wang [18] for a binary option, cash-or-nothing type, with $s_{\max}=700$, $K=400$, $\sigma=0.4$, $r=0.1$, $d=0.04$ and $N=M=100$. The result is presented in Fig. 4. As we observe, even when the initial data is discontinuous, no spurious oscillations appear in the solution.

Despite of convenient properties of this method, problems arise for high Péclet numbers during the numerical simulation. In the definitions (4.10)-(4.11) the variable s has as exponent the term

$$\alpha_i=\frac{b(s_i,t)}{a(t)}=2\frac{r(t)-\sigma^2(t)}{\sigma^2(t)}$$

and for the case $\sigma^2\ll r$ we have that $\alpha_i=\mathcal{O}(r/\sigma^2)$, i.e., the Péclet number and α_i are of the same order. In the example shown in Fig. 4 we have $\alpha=-1.25$, whereas for the case considered in Section 3.1, this value is $\alpha=998$.

Here, in the convection dominated case, the term in the denominator could be out of the range of representable numbers on a computer. Next, we modify the equations for $e_{i,i}$ stated in [18] in order to avoid the effect of subtractive cancellation for large Péclet numbers. In the definitions (4.10)–(4.11) terms of the form

$$\frac{s_i^{\alpha_i}}{s_{i+1}^{\alpha_i}-s_i^{\alpha_i}}$$

are recurrent, hence we write these terms as

$$\frac{1}{\left(\frac{s_{i+1}}{s_i}\right)^{\alpha_i}-1},$$

for instance. Now with $s_{i+1}:=s_i+\Delta s$ and using the binomial series expansion we get for the denominator

$$\left(\frac{s_i+\Delta s_i}{s_i}\right)^{\alpha_i}-1=\left(1+\frac{\Delta s_i}{s_i}\right)^{\alpha_i}-1=\sum_{k=1}^{\infty}\binom{\alpha_i}{k}\left(\frac{\Delta s_i}{s_i}\right)^k, \tag{4.15}$$

(with an appropriately truncated series in the implementation) which is more robust for the case of a high Péclet number. For practical purposes, it is possible to use Wang's FV scheme for the case of a large interval $s \in [s_{\min}, s_{\max}]$ and a relatively large $N \sim 10^5$, for example. However, the method is just order one and therefore does not represent any advantage over the EFM. from Subsection 3.1.

5 The Kurganov-Tadmor scheme

Kuganov and Tadmor [14] introduced a high resolution scheme for nonlinear conservation laws and convection-diffusion equations. The main idea here is to use more precise information of local propagation speeds at cell boundaries in order to average non-smooth parts of the computed approximation over smaller cells than in the smooth regions. By treating smooth and non-smooth regions separately the numerical diffusion introduced by the method is independent of Δt. We only highlight important points of it and state the final fully-discrete and semi-discrete scheme. To start, we consider (4.1) or the related convection-diffusion equation

$$\frac{\partial}{\partial t}u(x,t)+\frac{\partial}{\partial x}f(u(x,t))=\frac{\partial}{\partial x}Q(u(x,t),u_x(x,t)). \tag{5.1}$$

An admissible mesh of size $N+1$ is defined as in (4.2) with a family of equidistant points x_i and a family of midpoints $I_i=[x_{i-1/2},x_{i+1/2}]$. The step sizes Δx, Δt are defined as before. It is assumed that a piecewise, linear approximation

$$\tilde{u}(x,t_n)=\sum_i \big(U_i^n-(U_x)_i^n(x-x_i)\big)\mathbf{1}_{I_i}$$

at time level t_n is already computed based on cell averages U_i^n-for clarity, we omit here the bar notation to denote cell averages over the interval I_i-and the approximation to the derivative $(U_x)_i^n$. The upper bound of the local speed of propagation at the boundary of the cell $x_{i+1/2}$ for the nonlinear or linearly degenerate case is given by

$$a^n_{i+\frac{1}{2}}=\max\Big[\rho\Big(\frac{\partial}{\partial u}f(U^+_{i+\frac{1}{2}})\Big),\rho\Big(\frac{\partial}{\partial u}f(U^-_{i+\frac{1}{2}})\Big)\Big], \tag{5.2}$$

where

$$U^+_{i+\frac{1}{2}}=U^n_{i+1}-\frac{\Delta x}{2}(U_x)^n_{i+1},\qquad U^-_{i+\frac{1}{2}}=U^n_i+\frac{\Delta x}{2}(U_x)^n_i$$

are the corresponding left and right intermediate values of $\tilde{u}(x,t_n)$ at $x_{i+1/2}$ and $\rho(A)$ denotes the spectral radius of A.

Instead of averaging over the control volumes $I_i\times[t_n,t_n+\Delta t]$, this scheme performs the integration over variable control volumes $[x_{i+1/2,l},x_{i+1/2,r}]\times[t_n,t_n+\Delta t]$ where

$$x_{i+\frac{1}{2},l}=x_{i+\frac{1}{2}}-a^n_{i+\frac{1}{2}}\Delta t,\qquad x_{i+\frac{1}{2},r}=x_{i+\frac{1}{2}}+a^n_{i+\frac{1}{2}}\Delta t.$$

Due to the finite speed of propagation, the new interval differentiates between smooth and non-smooth regions providing the non-smooth parts with a narrower control volume of spatial width $2a^n_{i+1/2}\Delta t$.

Defining

$$\mathcal{I}_i=[x_{i+\frac{1}{2},l},x_{i+\frac{1}{2},r}] \quad \text{and} \quad \Delta x_{i+\frac{1}{2}}=x_{i+\frac{1}{2},r}-x_{i+\frac{1}{2},l}=2a^n_{i+\frac{1}{2}}\Delta t,$$

which denotes the width of the Riemann fan originating at $x_{i+1/2}$, and proceeding similar as before we obtain the cell averages at $t_n+\Delta t$ we can express (4.1) as

$$\begin{aligned}\frac{1}{\Delta x_{i+\frac{1}{2}}}\int_{\mathcal{I}_i}u(x,t_{n+1})dx=&\frac{1}{\Delta x_{i+\frac{1}{2}}}\int_{\mathcal{I}_i}\tilde{u}(x,t_n)dx-\frac{1}{\Delta x_{i+\frac{1}{2}}}\int_{t_n}^{t_n+\Delta t}f(u(x_{i+\frac{1}{2},r},t))\\&+\frac{1}{\Delta x_{i+\frac{1}{2}}}\int_{t_n}^{t_n+\Delta t}f(u(x_{i+\frac{1}{2},l},t))dt\end{aligned}\tag{5.3}$$

and similarly for the point x_i over the interval $\mathcal{I}^2_i=[x_{i+1/2,l},x_{i+1/2,r}]$ with $\Delta x_i=x_{i+1/2,l}-x_{i+1/2,r}=\Delta x-\Delta t(a^n_{i-1/2}+a^n_{i+1/2})$

$$\begin{aligned}\frac{1}{\Delta x_i}\int_{\mathcal{I}^2_i}u(x,t_{n+1})dx=&\frac{1}{\Delta x_i}\int_{\mathcal{I}^2_i}\tilde{u}(x,t_n)dx-\frac{1}{\Delta x_i}\int_{t_n}^{t_n+\Delta t}f(u(x_{i+\frac{1}{2},l},t))\\&+\frac{1}{\Delta x_i}\int_{t_n}^{t_n+\Delta t}f(u(x_{i+\frac{1}{2},r},t))dt.\end{aligned}\tag{5.4}$$

It is worthwhile noting that in the second term on the right hand side of (5.3) and (5.4), the flux is evaluated with the unknown function $u(x,t)$ whereas the first term is obtained via the known piecewise solution $\tilde{u}(x,t)$.

Eqs. (5.3) and (5.4) lead to the cell averages over the nonuniform grid $[x_{i+1/2,l},x_{i+1/2,r}]$

$$w^{n+1}_{i+\frac{1}{2}}=\frac{U^n_i+U^n_{i+1}}{2}+\frac{\Delta x-a^n_{i+\frac{1}{2}}\Delta t}{4}\left[(U_x)^n_i-(U_x)^n_{i+1}\right]-\frac{1}{2a^n_{i+\frac{1}{2}}}\left[f(U^{n+\frac{1}{2}}_{i+\frac{1}{2},r})-f(U^{n+\frac{1}{2}}_{i+\frac{1}{2},l})\right],$$

$$w^{n+1}_i=U^n_i+\frac{\Delta t}{2}(a^n_{i-\frac{1}{2}}-a^n_{i+\frac{1}{2}})(U_x)^n_i-\lambda\frac{f(U^{n+\frac{1}{2}}_{i+\frac{1}{2},l})-f(U^{n+\frac{1}{2}}_{i+\frac{1}{2},r})}{1-\lambda(a^n_{i-\frac{1}{2}}+a^n_{i+\frac{1}{2}})},$$

where $\lambda=\Delta t/\Delta x$ is the hyperbolic mesh ratio. Finally, the nonuniform averages are projected back to the uniform grid yielding the fully discrete, second-order scheme

$$\begin{aligned}U^{n+1}_i=&\lambda a^n_{i-\frac{1}{2}}w^{n+1}_{i-\frac{1}{2}}+\left[1-\lambda(a^n_{i-\frac{1}{2}}+a^n_{i+\frac{1}{2}})\right]w^{n+1}_i+\lambda a^n_{i+\frac{1}{2}}w^{n+1}_{i+\frac{1}{2}}\\&+\frac{\Delta x}{2}\left[(\lambda a^n_{i-\frac{1}{2}})^2(U_x)^{n+1}_{i-\frac{1}{2}}-(\lambda a^n_{i+\frac{1}{2}})^2(U_x)^{n+1}_{i+\frac{1}{2}}\right].\end{aligned}$$

The semi-discrete scheme is obtained by letting $\Delta t \to 0$ in the expressions for w_i^{n+1}, $w_{i+1/2}^{n+1}$ and U_i^{n+1}, cf. [14] for more details. The scheme reads

$$\frac{d}{dt}U_i(t) = -\frac{1}{\Delta x}\left[H_{i+\frac{1}{2}}(t) - H_{i-\frac{1}{2}}(t)\right] \tag{5.5}$$

with the numerical flux given by

$$H_{i\pm\frac{1}{2}}(t) = \frac{1}{2}\left[f(U^+_{i\pm\frac{1}{2}}(t)) + f(U^-_{i\pm\frac{1}{2}}(t))\right] - \frac{a_{i\pm\frac{1}{2}}(t)}{2}\left[U^+_{i\pm\frac{1}{2}}(t) - U^-_{i\pm\frac{1}{2}}(t)\right] \tag{5.6}$$

and the values $U^{\pm}_{i\pm\frac{1}{2}}(t)$ given by

$$\begin{aligned} U^-_{i-\frac{1}{2}}(t) &= U_{i-1}(t) + \frac{1}{2}\Delta x(U_x)_{i-1}(t), & U^+_{i+\frac{1}{2}}(t) &= U_{i+1}(t) - \frac{1}{2}\Delta x(U_x)_{i+1}(t), \\ U^-_{i+\frac{1}{2}}(t) &= U_i(t) + \frac{1}{2}\Delta x(U_x)_i(t), & U^+_{i-\frac{1}{2}}(t) &= U_i(t) + \frac{1}{2}\Delta x(U_x)_i(t). \end{aligned}$$

For completeness, we also state the semi-discrete analogue of (5.2)

$$a_{i+\frac{1}{2}}(t) = \max\left[\rho\Big(\frac{\partial}{\partial u}f(U^+_{i+\frac{1}{2}}(t))\Big), \rho\Big(\frac{\partial}{\partial u}f(U^-_{i+\frac{1}{2}}(t))\Big)\right]. \tag{5.7}$$

We can easily verify that (5.5) is a conservative method, i.e.,

$$H_{i+\frac{1}{2}}(t) \equiv H(U_{i-1}(t), U_i(t), U_{i+1}(t), U_{i+2}(t)).$$

The numerical viscosity, or artificial diffusion, introduced by this method is of order $\mathcal{O}(\Delta x^3)$ whereas for other schemes like the Lax-Friedrichs method it is $\mathcal{O}(\Delta x^2/\Delta t)$.

It is possible to extend the scheme (5.5) for convection-diffusion equations by including a reasonable numerical approximation for the dissipative flux denoted by $Q(u(x,t), u_x(x,t))$. The resulting scheme reads

$$\frac{d}{dt}U_i(t) = -\frac{1}{\Delta x}\left[H_{i+\frac{1}{2}}(t) - H_{i-\frac{1}{2}}(t)\right] + \frac{1}{\Delta x}\left[P_{i+\frac{1}{2}}(t) - P_{i-\frac{1}{2}}(t)\right]$$

with

$$P_{i+\frac{1}{2}}(t) = \frac{1}{2}\left[Q\Big(U_i(t), \frac{U_{i+1}(t) - U_i(t)}{\Delta x}\Big) + Q\Big(U_{i+1}(t), \frac{U_{i+1}(t) - U_i(t)}{\Delta x}\Big)\right].$$

It is well known that ODEs obtained by applying semi-discretization methods are always stiff. Moreover, they become arbitrarily stiff as $\Delta x \to 0$, cf. [9].

5.1 The Black-Scholes equation and the Kurganov-Tadmor scheme

Now, the Black-Scholes equation (3.1) is discretized according to the Kurganov-Tadmor scheme. We want to transform the Black-Scholes PDE to the general form

$$\frac{\partial}{\partial t}u(x,t)+\frac{\partial}{\partial x}\mathcal{F}(u)=\frac{\partial}{\partial x}\mathcal{Q}(u,u_x)+\mathcal{S}(x,t,u),$$

where $\mathcal{S}$ is the source term. To this end, the following expressions

$$\frac{\partial}{\partial s}(sv(s,t))=s\frac{\partial}{\partial s}v(s,t)+v(s,t),\qquad \frac{\partial}{\partial s}(s^2\frac{\partial}{\partial s}v(s,t))=s^2\frac{\partial^2}{\partial^2 s}v(s,t)+2s\frac{\partial}{\partial s}v(s,t)$$

can be used to get the Black-Scholes equation to the required form

$$\frac{\partial}{\partial t}v(s,t)+\frac{\partial}{\partial s}\big((\sigma^2-r+d)sv(s,t)\big)=\frac{\partial}{\partial s}\Big(\frac{\sigma^2}{2}s^2\frac{\partial}{\partial s}v(s,t)\Big)+(\sigma^2-2r+d)v(s,t).$$

Therefore, the fluxes are defined as

$$\mathcal{F}(s,v):=(\sigma^2-r+d)sv(s,t),\ \ \mathcal{Q}(s,v):=\frac{\sigma^2}{2}s^2\frac{\partial}{\partial s}v(s,t),\ \ \mathcal{S}(v):=(\sigma^2-2r+d)v(s,t).$$

The expression for $a_{i+1/2}(t)$ is simplified in this scalar case:

$$\frac{\partial}{\partial v}\mathcal{F}(s,v)\equiv\mathcal{F}_v=(\sigma^2-r+d)s,$$

i.e.,

$$a_{i+\frac{1}{2}}(t)=\big|\mathcal{F}_v(s_{i+\frac{1}{2}})\big|.$$

On the other hand, $\mathcal{Q}$ does not depend on $v(x,t)$ but only on the derivative $\partial v/\partial s$. Hence, the expression for P is also simplified, namely

$$P_{i+\frac{1}{2}}(t)=\mathcal{Q}\Big(\frac{V_{i+1}(t)-V_{i-1}(t)}{2\Delta s}\Big),$$

where the second-order approximation for the derivative is used. At the boundaries, we used the following second-order formulae to approximate the derivatives of $\mathcal{Q}$

$$\begin{aligned}\frac{\partial}{\partial s}v(s_{\min},t)&=\frac{-3V_0(t)+4V_1(t)-V_2(t)}{2\Delta s}+\mathcal{O}(\Delta s^2),\\ \frac{\partial}{\partial s}v(s_{\max},t)&=\frac{V_{N-1}(t)-4V_N(t)+3V_{N+1}(t)}{2\Delta s}+\mathcal{O}(\Delta s^2),\end{aligned}$$

where V_0 represents the approximation at $s_{\min}$ and V_{N+1} at $s_{\max}$.

The semi-discrete scheme for the Black-Scholes equation takes the form

$$\frac{dV_i}{dt}=-\frac{1}{\Delta s}\big[H_{i+\frac{1}{2}}(t)-H_{i-\frac{1}{2}}(t)\big]+\frac{1}{\Delta s}\big[P_{i+\frac{1}{2}}(t)-P_{i-\frac{1}{2}}(t)\big]+\mathcal{S}(v)$$

with

$$H_{i+\frac{1}{2}}(t)=\frac{1}{2}\Big[\mathcal{F}\big(s_{i+\frac{1}{2}},V^{+}_{i+\frac{1}{2}}\big)+\mathcal{F}\big(s_{i+\frac{1}{2}},V^{-}_{i+\frac{1}{2}}\big)\Big]-\frac{a_{i+\frac{1}{2}}(t)}{2}\big[V^{+}_{i+\frac{1}{2}}(t)-V^{-}_{i+\frac{1}{2}}(t)\big],$$
$$H_{i-\frac{1}{2}}(t)=\frac{1}{2}\Big[\mathcal{F}\big(s_{i-\frac{1}{2}},V^{+}_{i-\frac{1}{2}}\big)+\mathcal{F}\big(s_{i-\frac{1}{2}},V^{-}_{i-\frac{1}{2}}\big)\Big]-\frac{a_{i+\frac{1}{2}}(t)}{2}\big[V^{+}_{i-\frac{1}{2}}(t)-V^{-}_{i-\frac{1}{2}}(t)\big].$$

The derivative $(V_s)_i(t)$ is approximated with a minmod limiter such that the semi-discrete scheme fulfills the total variation diminishing (TVD) condition [14].

The generalized minmod limiter is defined as

$$(V_s)_i(t):=\text{minmod}\Big(\theta\frac{V_i(t)-V_{i-1}(t)}{\Delta s},\frac{V_{i+1}(t)-V_{i-1}(t)}{2\Delta s},\theta\frac{V_{i+1}(t)-V_i(t)}{\Delta s}\Big),\tag{5.8}$$

where $1\leq\theta\leq 2$ and the minmod function is defined as

$$\text{minmod}(x_1,x_2,\cdots,)=\begin{cases}\min_i(x_i), & \text{if } x_i>0, \quad \forall i,\\ \max_i(x_i), & \text{if } x_i<0, \quad \forall i,\\ 0, & \text{otherwise.}\end{cases}$$

6 Numerical simulations using the Kurganov-Tadmor scheme

6.1 European options

To test the KT scheme and its properties, a convection-dominated example with high Péclet number and known analytic solution is considered. Thus, $r=0.46$, $\sigma=0.02$, $d=0$, $K=70$, $s_{\min}=0$, $s_{\max}=100$ and $T=1$. Although this setup is financially unrealistic, it is useful as a stress-test. The value of the Péclet number is

$$Pe\propto\frac{r}{\sigma^2}=1150.$$

In the case of a European option with Dirichlet boundary conditions, these conditions are included in the calculation of the derivative. For example, for $i=1$ we have

$$(V_s)_1(t)=\text{minmod}\Big(\theta\frac{V_1(t)-g_{s_{\min}}(t)}{\Delta s},\frac{V_2(t)-g_{s_{\min}}(t)}{2\Delta s},\theta\frac{V_2(t)-V_1(t)}{\Delta s}\Big),$$

where $g_{s_{\min}}(t)$ represents the prescribed boundary condition at $s_{\min}$. A similar strategy is followed for the terms $V^{\pm}_{i+1/2}$. For instance

$$V^{-}_{1-\frac{1}{2}}=g_{s_{\min}}(t)+\frac{1}{2}\Delta s(V_s)_{i-1}(t).$$

The parameter θ is chosen problem-wise, e.g., $\theta=1$ ensures non-oscillatory behavior. We found empirically that the values $\theta\in[1.5,2]$ produce better results in this test example.

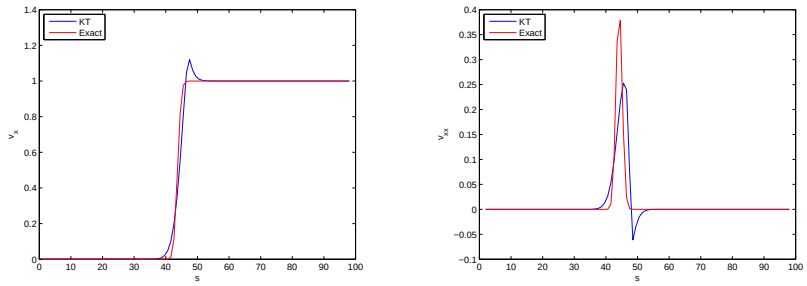

(a) First and second derivative of the price with $\theta=1$.

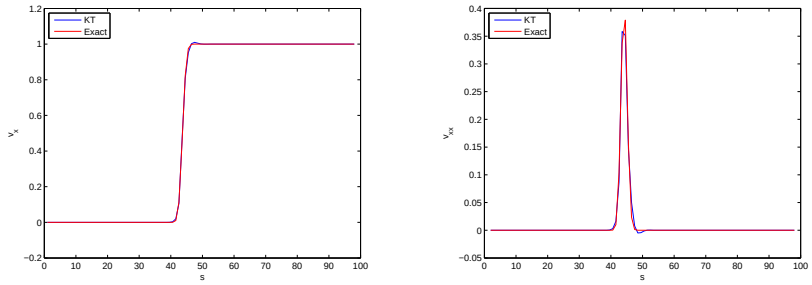

(b) First and second derivative of the price with $\theta=1.5$.

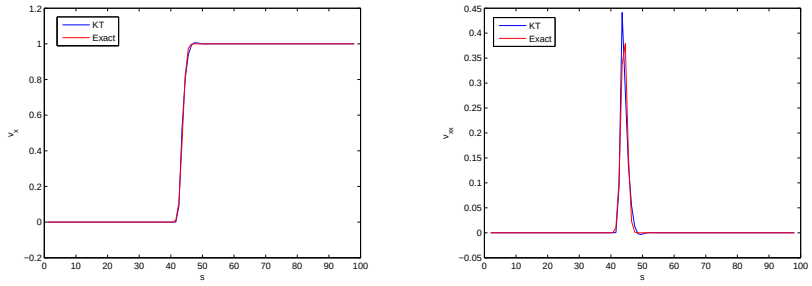

(c) First and second derivative of the price with $\theta=2$.

Figure 5: Results for different values of θ.

This behavior is also reported in [14] for the examples presented. To justify our selection for the value of θ, we present three cases with $N=100$ using an ODE integrator with automatic time step selection. From Fig. 5 it is observed that $\theta=1$ provides the worst result for both the first and the second derivative. For the first derivative, $\theta=2$ gives the best results but the second derivative is over estimated. The value $\theta=1.5$ is the best for both the first and the second derivative. We select $\theta=1.5$ for the minmod limiter for all the simulations and proceed with $N=500$, see Figs. 6 and 7. The approximation for the price is quite good and it is easily spotted that the approximation for the Δ and Γ is improving fast thanks to the order of convergence of the method, providing a high resolution both for the price and its derivatives.

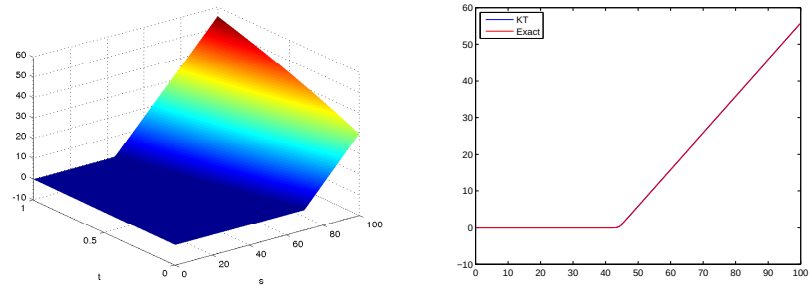

(a) Surface for $t \in [0,T]$. (b) Price at $t = T$.

Figure 6: Price of the option obtained via Kurganov-Tadmor scheme.

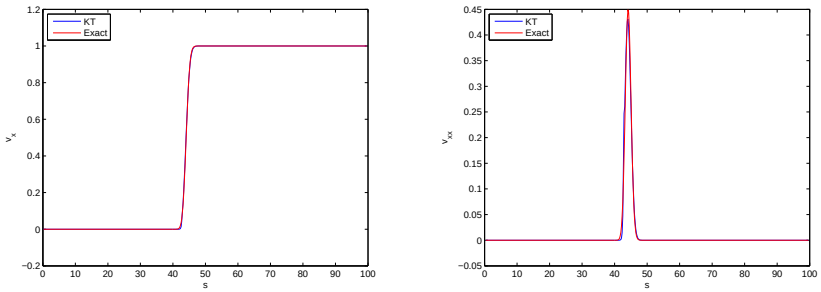

(a) First derivative Δ. (b) Second derivative Γ.

Figure 7: Greeks of the option price.

Results of the computational order of convergence for Kurganov-Tadmor scheme, measured with the Euclidean norm, are shown in Table 2. It can be seen that the computational convergence behaves as predicted theoretically.

The KT scheme delivers excellent approximations for the benchmark problem. The first derivative Δ of the approximation of the price is now free of oscillations and it is easily observed that almost no artificial diffusion is introduced. The second derivative is shown in Fig. 7(b). Thanks to the resolution achieved with the KT scheme, the second derivative of the approximation is remarkably good. In other cases like the EFM, due to the artificial diffusion introduced by the method, the second derivative is already quite a deficient approximation even if the first derivative is acceptable. It can be seen that the KT scheme represents a big advantage in comparison to other schemes avail-

Table 2: Error in the price of a European option obtained via KT scheme.

N	300	400	500	600	700
$\|v(s,T)-V_i^M\|_2$	0.066468	0.054178	0.041912	0.032635	0.026116
Δs^2	0.110374	0.062189	0.039840	0.027685	0.020350

able for two reasons: the convergence properties and its flexibility. Discontinuities and non-smoothness on the initial data are handled satisfactorily.

We now proceed to test the Kurganov-Tadmor scheme with option pricing equations that present hyperbolic behavior even for realistic parameters.

6.2 Asian options

Here we consider (2.4) for the numerical pricing of an Asian option. We perform a time reversal $t^*=T-t$ but, again, for convenience we simply denote t^* as t:

$$\frac{\partial v}{\partial t}=\frac{1}{2}\sigma^2 s^2\frac{\partial^2 v}{\partial s^2}+rs\frac{\partial v}{\partial s}-ru+\frac{1}{T-t}(s-a)\frac{\partial v}{\partial a} \tag{6.1}$$

with boundary conditions

$$\frac{\partial v}{\partial t}=-\frac{a}{T-t}\frac{\partial v}{\partial a}-rv \quad \text{for } s=0, \tag{6.2a}$$

$$\frac{\partial v}{\partial t}=\frac{s_{\max}-a}{T-t}\frac{\partial v}{\partial a} \quad \text{for } s=s_{\max}. \tag{6.2b}$$

The Kurganov-Tadmor scheme is easily extended to two spatial dimensions [14]. The scheme takes the form

$$\begin{aligned}\frac{dV_{i,j}(t)}{dt}=&-\frac{1}{\Delta s}\left[H^s_{i+\frac{1}{2},j}(t)-H^s_{i-\frac{1}{2},j}(t)\right]-\frac{1}{\Delta a}\left[H^a_{i,j+\frac{1}{2}}(t)-H^a_{i,j-\frac{1}{2}}(t)\right]\\&+\frac{1}{\Delta s}\left[P^s_{i+\frac{1}{2},j}(t)-P^s_{i-\frac{1}{2},j}(t)\right]+\frac{1}{\Delta a}\left[P^a_{i,j+\frac{1}{2}}(t)-P^a_{i,j-\frac{1}{2}}(t)\right]\end{aligned}$$

with the usual definitions for $H(t)$ and $P(t)$.

By following the same technique as in Section 6.1, the convective fluxes for the Eq. (6.1) are found to be:

$$\mathcal{F}^s(s,v)=(\sigma^2-r)sv, \qquad \mathcal{F}^a(s,a,v)=-\frac{1}{T-t}(s-a)v.$$

On the other hand, there is diffusion flux only for the spatial direction s

$$\mathcal{Q}^s(s,v,v_s)=\frac{1}{2}\sigma^2 s^2\frac{\partial v}{\partial s}$$

and finally, the source is

$$\mathcal{S}=(\sigma^2-2r+\frac{1}{T-t})v.$$

Boundary conditions are of Neumann type. Including expressions (6.2a) and (6.2b) into the discretization is not easy because the expressions H^s and H^a are elaborated. Nevertheless, we noticed that those expressions are analytically solvable and their exact solutions are defined uniquely by the initial condition, i.e., the payoff. The boundaries for

a fixed strike Asian put option are:

$$v(0,a,t) = \max\left(0, K - \frac{1}{T}(T-t)a\right)\exp(-rt),$$
$$v(s_{\max},a,t) = \max\left(0, K - \frac{1}{T}[s_{\max}t + a(T-t)]\right).$$

For the expression (6.2b) an analytic solution is obtained and for expression (6.2a), a transformation is needed. By defining $\tilde{v} = v\exp(rt)$ and substituting it into the PDE, the boundary condition takes the form

$$\frac{\partial \tilde{v}}{\partial t} = \frac{a}{T-t}\frac{\partial \tilde{v}}{\partial a},$$

which is now easily solved. An inverse transformation to get the original variable v back is straightforward obtained.

An example from [17] for a fixed strike put is shown in Fig. 8 with $K = 100$, $T = 0.2$, $r = 0.05$, $\sigma = 0.25$ and $N = 50$, $\theta = 1.5$, $s_{\min} = a_{\min} = 0$ and $s_{\max} = a_{\max} = 200$. The simulation for $t = 0.06$ is performed with an ODE solver with automatic time step size selection. The final price and its derivative is shown in Fig. 9.

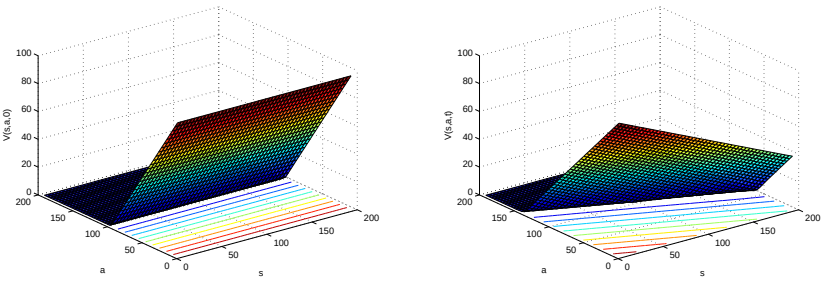

(a) Initial Condition. (b) Price at $t = 0.06$.

Figure 8: Simulation of a fixed strike Asian option with the KT scheme.

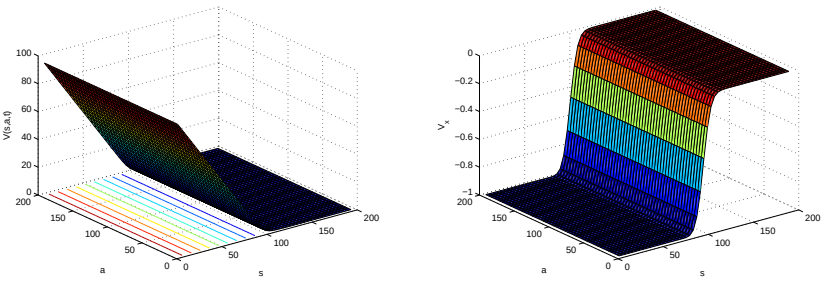

(a) Price. (b) Derivative.

Figure 9: Simulation of a fixed strike Asian option at $t = T$.

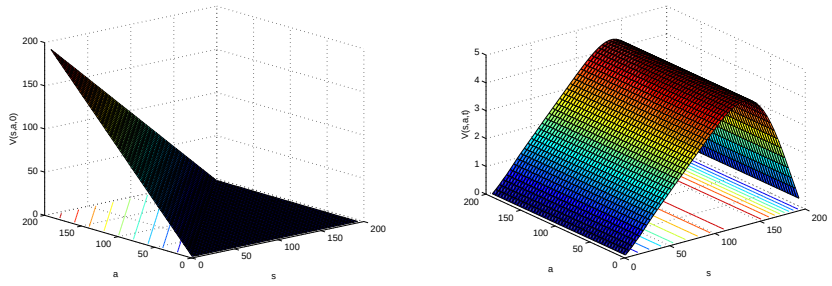

(a) Initial Condition. (b) Price at $t=T$.

Figure 10: Floating strike Asian option.

Next we present the case of a floating strike put option with $r=0.15$, $\sigma=0.3$, $T=1$ and $N=50$. The IC is $v(s,a,0)=(a-s)^+$ and the BCs take the form

$$v(0,a,t)=\max\left(0,-s_{\min}+\frac{1}{T}(T-t)a\right)\exp(-rt),$$
$$v(s_{\max},a,t)=\max\left(0,-s_{\max}+\frac{1}{T}\left[s_{\max}t+a(T-t)\right]\right).$$

The final price along with the initial condition is shown in Fig. 10. The derivative in this case shows some oscillation near $s=0$, as shown in Fig. 11.

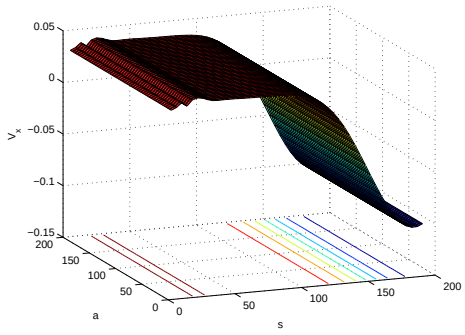

Figure 11: Floating strike Asian option price derivative at $t=T$.

In this case, the computational cost is much higher than in the simulation of an European option, since for Asian options, the ODE solver is handling systems of size N^2.

6.3 Wilmott reduction for asian options

In Section 2.3 a reduction of the full PDE (2.4) for floating strike Asian options was presented. As in other sections, the PDE is expressed in forward-in-time form first and then the convective and diffusive fluxes are obtained, if any. This PDE is convection-dominated for small σ as well as for $x\approx 0$.

Table 3: Floating-strike Asian put comparison with values from [15, Table 5], $s=100$.

σ	r	NAG-RS	KT-Wilmott	LB	UB
0.1	0.05	1.257	*1.441	1.245	1.355
	0.09	0.709	0.817	0.699	0.825
	0.15	0.271	0.294	0.252	0.415
0.2	0.05	*3.401	3.656	3.404	3.831
	0.09	2.622	2.826	2.622	3.062
	0.15	1.723	1.855	1.710	2.187
0.3	0.05	5.628	5.902	5.625	6.584
	0.09	*4.736	4.980	4.738	5.706
	0.15	3.612	3.803	3.609	4.604

The forward-in-time PDE takes the form

$$\frac{\partial y}{\partial t}=\frac{1}{2}\sigma^2x^2\frac{\partial^2 y}{dx^2}+(1-rx)\frac{\partial y}{\partial x},\quad x>0,\quad t>0, \tag{6.3}$$

where the IC for a call is $y(x,0)=(1-x/T)^+$. The BC (2.9) for $x=0$ takes the form $\partial y/\partial t=\partial y/\partial x$ and $y=0$ for $x\to\infty$. As in Section 6.2 the BCs are solved analytically when possible. Then the unknown BCs for put options are obtained via the put-call parity.

The fluxes for the PDE (6.3) are determined analogously and read

$$\mathcal{F}=-(1-rx-\sigma^2x)y,\qquad \mathcal{Q}=\frac{1}{2}\sigma^2x^2y,\qquad \mathcal{S}=(\sigma^2+r)y.$$

Table 3 shows a comparison of the results obtained in [15] for a floating-strike Asian put and $s=100$ and the results obtained with the Wilmott PDE discretized with the Kurganov-Tadmor scheme.

The results provided by Rogers and Shi were obtained with the NAG routine D03PAF with Δx=0.005 and are listed in column NAG-RS. The columns LB and UB displays lower and upper bounds for the numerical solution. The column KT-Wilmott corresponds to the approximation obtained with the Kurganov-Tadmor scheme with the same step size. For fixed Δx we observe slightly different approximations between the two schemes. The results highlighted with a star are outside the boundaries. For this example it can be observed that in general both schemes usually deliver approximation within bounds. It is also clear that the Kurganov-Tadmor scheme provides approximations that are always higher than those provided by the NAG routine D03PAF.

In Table 4 a list of results for a floating-strike Asian call is shown. The comparison is between a Crank-Nicolson implicit method (CN), a high order compact scheme (HOC), a Monte Carlo (MC) method proposed in [13] versus the Kurganov-Tadmor scheme using the Wilmott (KT-W) PDE, all of them with $N=500$. It is easy to spot that the worst performer is the CN scheme providing approximations far away from the other three schemes whereas the HOC scheme results are similar to those obtained with the Kurganov-Tadmor scheme. It is interesting to note that the largest deviation between

Table 4: Floating-strike Asian call option comparison with prices in [13, Table 1 and 2].

σ	r	CN	HOC	MC	KT-W
0.05	0.06	3.5025	3.1391	3.1509	2.9686
	0.1	5.1148	4.8784	4.8734	4.6809
	0.2	9.3988	9.3449	9.3486	9.2018
0.1	0.06	4.1353	3.8929	4.0124	3.8955
	0.1	4.0124	5.3592	5.4183	5.2841
	0.2	9.5333	9.4385	9.433	9.2962
0.2	0.06	6.1337	5.9919	6.1172	6.0316
	0.1	7.2951	7.1641	7.2625	7.1731
	0.2	10.547	10.4486	10.4894	10.3942
0.3	0.06	8.3256	8.2462	8.3155	8.2404
	0.1	9.3669	9.2902	9.3484	9.2735
	0.2	12.2035	12.1361	12.163	12.0931
0.4	0.06	10.5403	10.4921	10.5358	10.4614
	0.1	11.5081	11.4607	11.4952	11.4244
	0.2	14.0885	14.0444	14.0581	13.9955

HOC and KT-W columns occurs. in the case of a small volatility, i.e., $\sigma = 0.05$. Furthermore, it can be seen that in convection-dominated environments, the columns CN, HOC and MC are similar in contrast to the approximation obtained with Kurganov-Tadmor-observe, for example, the case for $\sigma = 0.05$ and $r = 0.2$. It is expected that the CN method is affected by the convective behavior and, judging by the results listed in Table 4, it might be possible that the HOC is also affected.

6.4 Rogers-Shi reduction for asian options

Here a simulation of the Rogers-Shi PDE reduction presented in Section 2.4 with the Kurganov-Tadmor scheme is performed. This PDE is convection dominated for small σ and for short maturity times T. The forward-in-time PDE reads

$$\frac{\partial w}{\partial t} = \frac{1}{2}\sigma^2 x^2 \frac{\partial^2 w}{\partial x^2} - (\rho(t) + rx)\frac{\partial w}{\partial x}$$

and the boundary conditions are changed accordingly. The fluxes are

$$\mathcal{F} = (\rho(t) + rx + \sigma^2 x)w, \qquad \mathcal{Q} = \frac{1}{2}\sigma^2 x^2 \frac{\partial w}{\partial x}, \qquad \mathcal{S} = (\sigma^2 + r)w$$

and $\rho(t)$ is defined depending on the type of the Asian option: fixed or floating strike.

A comparison of the data in [15] and the prices obtained with the Kurganov-Tadmor scheme is shown in Table 5. The column RS refers to the results of a fixed strike Asian call option presented by Rogers-Shi with the NAG routine D03PAF with $\Delta x = 0.005$, $s = 100$ and $\sigma = 0.05$. The column KT1 shows the results obtained with the Kurganov-Tadmor scheme with the same step-size. The column KT2 is a simulation with $\Delta x = 0.00125$.

Table 5: Comparison of the results from [15, Table 1] vs. the Kurganov-Tadmor scheme.

r	Strike	RS	KT1	KT2	LB	UB
0.05	95	*7.157	7.180	7.178	7.174	7.183
	100	*2.621	*2.742	2.719	2.713	2.722
	105	*0.439	*0.311	0.334	0.337	0.343
0.09	95	8.823	8.809	8.809	8.809	8.821
	100	*4.185	*4.324	4.311	4.308	4.318
	105	*1.011	0.958	0.958	0.958	0.968
0.15	95	*11.090	11.094	11.094	11.094	11.114
	100	*6.777	6.796	6.795	6.794	6.810
	105	*2.639	*2.768	2.747	2.744	2.761

Table 6: Data corresponding to [2, Table 3].

σ	K	Exact	Hsu-Lyuu		Chen-Lyuu		KT	
0.05	95	8.8088392	8.808717	$1.22e-04$	8.808839	$2.00e-07$	8.808983	$1.44e-04$
	100	4.3082350	4.309247	$1.01e-03$	4.308231	$4.00e-06$	4.318153	$9.92e-03$
	105	0.9583841	0.960068	$1.68e-03$	0.958331	$5.31e-05$	0.957513	$8.71e-04$
0.1	95	8.9118509	8.912238	$3.87e-04$	8.911839	$1.19e-05$	8.914974	$3.12e-03$
	100	4.9151167	4.914254	$8.63e-04$	4.915075	$4.17e-05$	4.920286	$5.17e-03$
	105	2.0700634	2.072473	$2.41e-03$	2.069930	$1.33e-04$	2.069732	$3.31e-04$
0.2	95	9.9956567	9.995661	$4.30e-06$	9.995362	$2.95e-04$	9.997251	$1.59e-03$
	100	6.7773481	6.777748	$4.00e-04$	6.776999	$3.49e-04$	6.778434	$1.09e-03$
	105	4.2965626	4.297021	$4.58e-04$	4.295941	$6.22e-04$	4.296475	$8.76e-05$
0.3	95	11.6558858	11.656062	$1.76e-04$	11.654758	$1.13e-03$	11.656542	$6.56e-04$
	100	8.8287588	8.829033	$2.74e-04$	8.827548	$1.21e-03$	8.829166	$4.07e-04$
	105	6.5177905	6.518063	$2.72e-04$	6.516355	$1.44e-03$	6.517857	$6.65e-05$
0.4	95	13.5107083	13.510861	$1.53e-04$	13.507892	$2.82e-03$	13.511028	$3.20e-04$
	100	10.9237708	10.923943	$1.72e-04$	10.920891	$2.88e-03$	10.923937	$1.66e-04$
	105	8.7299362	8.730102	$1.66e-04$	8.726804	$3.13e-03$	8.729934	$2.20e-06$
0.5	95	15.4427163	15.442822	$1.06e-04$	15.437069	$5.65e-03$	15.442907	$1.91e-04$
	100	13.0281555	13.028271	$1.15e-04$	13.022532	$5.62e-03$	13.028286	$1.30e-04$
	105	10.9296247	10.929736	$1.11e-04$	10.923750	$5.87e-03$	10.929685	$6.03e-05$
0.6	95		17.406402		17.396428		17.406609	
	100		15.128426		15.118595		15.128486	
	105		13.113874		13.103855		13.113802	
0.8	95		21.349949		21.326144		21.349981	
	100		19.288780		19.265518		19.288744	
	105		17.423935		17.400803		17.423820	
1.0	95		25.252051		25.205238		25.252053	
	100		23.367535		23.321951		23.367513	
	105		21.638238		21.593393		21.638200	

Looking at the column KT1 we notice that most of the time the Kurganov-Tadmor scheme yields results that are very close to or between the bounds. In contrast, the approximations on column RS are either above or below the interval defined by the bounds in all cases. Again, a star is placed to highlight a result if it is either up or down the interval defined by the bounds. It is remarkable that when comparing the approximations in column KT1 for different values of r, the Kurganov-Tadmor scheme produces better

results when the convective behavior is dominant, i.e., for the case when $r=0.15$ all our approximations in column KT1 are inside the bounds.

We list column KT2 with a grid four times finer than KT1 to show the convergence of the method. The simulation is achieved in approximately 1.5 minutes. In column KT2 all the approximations are inside the bounds. It is reported in [15] that as r increases, a rise in the simulation time is observed as well. Depending on the algorithm used, it could be expected that increasing r, leaving σ fixed, results in an increase on the simulation time because the convection-dominated behavior arises. This increase in simulation time is not observed with the Kurganov-Tadmor scheme.

Table 6 list a comparison of price of a fixed-strike Asian call option with $r=0.09$ obtained with the Kurganov-Tadmor scheme against two other approximations: the column labeled as "Chen-Lyuu" lists prices obtained with the method proposed in [2] which is a lower bound for the price. The values listed in column "Hsu-Lyuu" were obtained with lattice algorithm that exhibit quadratic-time convergence proposed in [11]. The column labeled as "Exact" is obtained with a semi-analytic method proposed in [21]. As Chen and Lyuu pointed out, the reason for testing the method with such large volatilities is because many formulas and numerical schemes deteriorate its approximation as the volatility increases. At the right-hand side of each approximation we provide the difference between the price obtained and the exact value. From this error we observe that the Kurganov-Tadmor scheme gives similar approximations to those obtained by the Hsu-Lyuu lattice algorithm. We also observe that the Chen-Lyuu formula does deteriorate with as the volatility is increased whereas the performance of the the Hsu-Lyuu lattice and the Kurganov-Tadmor scheme are stable for all σ.

7 Application to a nonlinear Black-Scholes equation

Finally, we consider a nonlinear Black-Scholes equation [1, 6] proposed by Windcliff et al. [20]. This nonlinear PDE arises when hedging a contingent claim with an asset that is not perfectly correlated with the underlying asset, e.g., the contingent claim is written on an asset with price s that cannot be traded. Instead, a reference, correlated asset is used to price the option. To be self-contained, we state here the most important details from [20]. To do so, let us define ρ as the correlation between the underlying asset and the reference, λ as the *risk loading parameter* and

$$q=\begin{cases}\operatorname{sign}\left(\dfrac{\partial v}{\partial s}\right), & \text{for a short position,}\\ -\operatorname{sign}\left(\dfrac{\partial v}{\partial s}\right), & \text{for a long position,}\end{cases}$$

then the nonlinear Black-Scholes takes the form

$$\frac{\partial v}{\partial t}=\max_{q\in[-1,1]}\left[\left(r'+q\lambda\sigma\sqrt{1-\rho^2}\right)s\frac{\partial v}{\partial s}+\frac{1}{2}\sigma^2s^2\frac{\partial^2 v}{\partial s^2}-rv\right] \tag{7.1}$$

for a short position and

$$\frac{\partial v}{\partial t}=\min_{q\in[-1,1]}\left[\left(r'+q\lambda\sigma\sqrt{1-\rho^2}\right)s\frac{\partial v}{\partial s}+\frac{1}{2}\sigma^2s^2\frac{\partial^2 v}{\partial s^2}-rv\right] \tag{7.2}$$

for a long position. The term r' is a function of the drift rate μ of the stochastic process driving the asset S and reference asset's drift rate μ', namely $r'=\mu-(\mu'-r)\sigma\rho/\sigma'$ with σ' defined as the volatility of the reference asset.

The boundary conditions are

$$\frac{\partial v}{\partial t}=-rv \quad \text{for } s\to 0, \tag{7.3a}$$

$$v=As\exp\left(\left(r'-r+q\lambda\sigma\sqrt{1-\rho^2}\right)t\right)+B\exp(-rt) \quad \text{for } s\to\infty, \tag{7.3b}$$

where A and B depend on the initial data, i.e., the payoff.

For discretization purposes we can write Eqs. (7.1) and (7.2) as

$$\frac{\partial v}{\partial t}=\left(r'+q\lambda\sigma\sqrt{1-\rho^2}\right)s\frac{\partial v}{\partial s}+\frac{1}{2}\sigma^2s^2\frac{\partial^2 v}{\partial s^2}-rv.$$

The fluxes are

$$\mathcal{F}=-\left(r'+q\lambda\sigma\sqrt{1-\rho^2}-\sigma^2\right)sv,\quad \mathcal{Q}=\frac{1}{2}\sigma^2s^2\frac{\partial v}{\partial s},\quad \mathcal{S}=\left(\sigma^2-r'-q\lambda\sigma\sqrt{1-\rho^2}\right)v,$$

which is all we need to define to apply the Kurganov-Tadmor scheme.

As an example, we perform a simulation with a short straddle option with the parameters: $r=0.05$, $\rho=0.9$, $\sigma=0.2$, $\mu=0.07$, $\sigma'=0.3$, $\mu'=r+(\mu-r)\sigma'\rho/\sigma=0.077$, $\lambda=0.2$, $r'=\mu-(\mu'-r)\sigma\rho/\sigma'=0.0538$, $K=100$, $T=1$. The payoff is

$$v(s,0)=(K-s)^+ +(s-K)^+$$

and the boundary conditions are

$$v(s_{\min},t)=K\exp(-rt)$$

for $s_{\min}$. For $s_{\max}$ at $t=0$ we have from (7.3b) that

$$\begin{aligned}&(K-s_{\max})^+ +(s_{\max}-K)^+ = As_{\max}\exp(0)+B\exp(0),\\ &s_{\max}-k=As_{\max}+B,\end{aligned}$$

therefore $A=1$ and $B=-K$ and the boundary condition at $s_{\max}$ is

$$v(s_{\max},t)=s_{\max}\exp\left(\left(r'-r+q\lambda\sigma\sqrt{1-\rho^2}\right)t\right)-K\exp(-rt).$$

Table 7: Comparison of CN scheme vs. KT method with the first set of parameters.

N	CN	KT
51	17.10144	17.92125
101	17.12367	17.98633
201	17.12899	18.00273
401	17.13021	18.00702
801	17.13050	18.00799
1601	17.13058	18.00817

Table 8: CN method vs. KT scheme for different stock values with $N=401$.

s	CN	KT
10	91.2063	93.9848
20	85.3930	87.9937
30	79.7849	82.2132
100	102.8771	103.9016

A comparison of the results presented in [20] and our results obtained with the Kurganov-Tadmor scheme is shown in Table 7 for $s=100$ and $t=T$. In the column labeled as "CN", the result obtained with Crank-Nicolson proposed by Windcliff is shown whereas the column "KT" is the price obtained with Kurganov-Tadmor scheme. A small discrepancy is between the CN method and the KT scheme is evident.

Nevertheless, the numerical method proposed by Windcliff is achieved with a standard central, forward or backward difference formula, i.e., the first derivative is-following Windcliff notation [20]-approximated as

$$(V_s)^n_{i,\text{cent}} = \frac{V^n_{i+1} - V^n_{i-1}}{s_{i+1} - s_{i-1}}$$

for the central difference case-cf. [20, Appendix A] for a detailed description of the method used to obtain the values in column CN.

As mentioned before, it is known that this schemes present issues due to the non-smoothness of the initial data and the convection-dominated behavior. Moreover, the numerical viscosity introduced by the central scheme is $\mathcal{O}(\Delta x^{2p}/\Delta t)$, where p is the order of convergence, which is higher than the viscosity introduces by the Kurganov-Tadmor method.

Next, we considered a short straddle but different set of parameters: $r=0.03$, $\rho=0.5$, $\sigma=0.7$, $\mu=0.04$, $\sigma'=0.25$, $\mu'=r+(\mu-r)\sigma'\rho/\sigma=0.0317$, $\lambda=0.9$, $r'=\mu-(\mu'-r)\sigma\rho/\sigma'=0.0375$, $K=100$, $T=1$. The corresponding list of numerical approximations is shown in Table 8. As expected, a discrepancy between both methods also appears for the second set of parameters.

Since we do not have any exact formula to compare with, we calculate the computational order of convergence (CC) by observing the error reduction when the number of grid points increase. Using the first set of parameters, the results are shown in Table 9.

Table 9: Computational convergence of the KT scheme.

N	KT	Error	CC
21	17.39550		
41	17.87244	0.47694	
81	17.97490	0.10245	4.6552
161	17.99992	0.02503	4.0941
321	18.00607	0.00615	4.0696
641	18.00759	0.00152	4.0405
1281	18.00801	0.00041	3.7027
2561	18.00810	0.00010	4.1797

Let V_1 be the approximation at s_i and T with N_1 discretization points and V_2 the approximation with N_2 for $N_1 < N_2$, then the error column in Table 9 is defined as

$$e = |V_1 - V_2|$$

and the column labeled as "CC" represents the computational order of convergence. As expected, in our numerical simulations, the Kurganov-Tadmor scheme exhibits quadratic convergence, i.e., by doubling the step-size, the error is decreased by a factor of 4.

8 Conclusions and outlook

In this work we compared three numerical methods to solve Black-Scholes type PDEs in the convection-dominated case. Up to the authors' knowledge it is the first time the Kurganov-Tadmor scheme is used for option pricing.

The exponentially fitted scheme is of order one and artificial diffusion is introduced as can be seen in Figs. 3(a) and 3(b). Near the strike price of the option, it is evident that the approximation is deficient due to the artificial diffusion.

Wang's fitted finite volume method of Section 4 is a robust method as it was shown with an example with discontinuous payoff: no oscillations are present. Wang's method is also of order one but the method in its original formulation cannot handle high Péclet numbers. We proposed a modification to solve this issue.

Extensive experiments and comparisons were made with the Kurganov-Tadmor scheme of Section 5. This method exhibits an advantageous convergence order of two, which is achieved even for the nonlinear Black-Scholes equation, cf. Table 9.

It was found that the flexibility of Kurganov-Tadmor scheme is very convenient for the pricing problem when different PDEs are used: by transforming the pricing PDE to the general convection-diffusion equation (5.1). Another advantage of the Kurganov-Tadmor scheme is that the numerical viscosity introduced by the scheme is only $\mathcal{O}(\Delta x)^{2p-1}$ where p is the order of convergence, whereas other central schemes introduce numerical viscosity $\mathcal{O}(\Delta x/\Delta t)^{2p}$. This characteristic allows to obtain a semi-discrete expression of the method by letting $\Delta t \to 0$ and take advantage of the existing

methods to solve ODEs numerically. However, one disadvantage of the semi-discrete form of the Kurganov-Tadmor scheme is that the resulting ODE system is stiff leading to a higher computational effort.

In Table 4 the same PDE with the Kurganov-Tadmor scheme was compared to other three methods with data from [13]. In this table it is evident the advantages of having a proper scheme for convection dominated PDEs. By comparing with the Crank-Nicolson column it is possible to spot the difference. The other two methods lead to similar results as those obtained with the Kurganov-Tadmor scheme.

The Rogers-Shi reduction was also compared to other numerical schemes techniques. In Table 5 the approximations with the Kurganov-Tadmor scheme are listed. We note that this method delivers better approximations – being a good approximation the one that is inside the bounds – in comparison to the scheme used in [15]. If we use a finer grid, then the power of the scheme is evident: all the approximations converge to values inside the interval between LB and UP. The Table 6 provides plenty of data to compare with. We observe that the Kurganov-Tadmor scheme does not lose accuracy when the volatility is increased, as reported in [2].

Finally, a nonlinear Black-Scholes PDE proposed in [20] was simulated. Comparisons are shown in Table 7 for the first set of parameters. The difference between the method proposed-a Crank-Nicolson method-and the Kurganov-Tadmor is significant. The Kurganov-Tadmor scheme performs adequately at discontinuities or non-smooth parts of the initial condition in the case of the benchmark problem.

However, the three schemes of this work do not possess the positivity preserving property for the computed price. This important property can be conserved e.g., by positive difference schemes [4] or special nonstandard schemes [7] and will be subject of future research.

Since the Black-Scholes differential operator degenerates at $s=0$, in fact a Dirichlet type boundary condition is often not a proper condition. For example, following the Fichera-Oleinik and Radkevich theory [10] setting in (2.2) $s=0$ we obtain

$$\frac{\partial v(0,t)}{\partial t} - rv(0,t) = 0 \quad t \in [0,T].$$

Solving this ODEs one can obtain for a vanilla put option the boundary condition at $s=0$, instead of using

$$v(s,t) = K\exp(-r(T-t)) - s\exp(-d(T-t)), \quad \text{for } s \to 0,$$

Chernogorova and Valkov [3] proposed recently a modification the Wang discretization [18] that adequately treats the proper (natural) boundary conditions for the zero-coupon degenerate parabolic equation. The same question of proper boundary conditions arises for Asian options, see (2.7) and the boundary condition (2.9). In a future work we will compare this modified Wang scheme [3] with the three numerical methods presented here.

References

[1] J. ANKUDINOVA AND M. EHRHARDT, *On the numerical solution of nonlinear Black-Scholes equations*, Comput. Math. Appl., 56 (2008), pp. 799–812.

[2] K. W. CHEN AND Y. D. LYUU, *Accurate pricing formulas for Asian options*, Appl. Math. Comput., 188 (2007), pp. 1711–1724.

[3] T. CHERNOGOROVA AND R. VALKOV, *Finite volume difference scheme for a degenerate parabolic equation in the zero-coupon bond pricing*, Math. Comput. Model., 54 (2011), pp. 2659–2671.

[4] A. DANG QUANG AND M. EHRHARDT, *Adequate numerical solution of air pollution problems by positive difference schemes on unbounded domains*, Math. Comput. Model., 44 (2006), pp. 834–856.

[5] D. DUFFY, Finite Difference Methods in Financial Engineering: A Partial Differential Equation Approach, Wiley, 2006.

[6] M. EHRHARDT, Nonlinear Models in Mathematical Finance: New Research Trends in Option Pricing, Nova Science Publishers, Inc., Hauppauge, NY 11788, 2008.

[7] M. EHRHARDT AND R. E. MICKENS, *A nonstandard finite difference scheme for convection-diffusion equations having constant coefficients*, Appl. Math. Comput., 219 (2013), pp. 6591–6604.

[8] R. EYMARD, T. GALLOUËT AND R. HERBIN, *Finite volume methods, Solution of Equation in* $\mathbb{R}^n$ *(part 3)*, Techniques of Scientific Computing (Part 3) (P. G. Ciarlet and J. L. Lions, eds.), Handbook of Numerical Analysis, Elsevier, 7 (2000), pp. 713–1018.

[9] C. GROSSMANN, H. G. ROOS AND M. STYNES, Numerical Treatment of Partial Differential Equations, Springer-Verlag, 2007.

[10] T. B. GYULOV AND R. L. VALKOV, Classical and Weak Solutions for Two Models in Mathematical Finance, Proceedings of the 37th International Conference Applications of Mathematics in Engineering and Economics (AMEE '11), June 8-13, 2011, Sozopol, Bulgaria, AIP Conf. Proc., 1410, pp. 195–202.

[11] W. W. Y. HSU AND Y. LYUU, *A convergent quadratic-time lattice algorithm for pricing European-style Asian options*, Appl. Math. Comput., 189 (2007), pp. 1099–1123.

[12] A. M. IL'IN, *Differencing scheme for a differential equation with a small parameter affecting the highest derivative*, Math. Notes, 6 (1969), pp. 596–602.

[13] A. KUMAR, A. WAIKOS AND S. P. CHAKRABARTY, *Pricing of average strike Asian call option using numerical PDE methods*, Int. J. Pure Appl. Math., 76 (2012), pp. 709–725.

[14] A. KURGANOV AND E. TADMOR, *New high-resolution central schemes for nonlinear conservation laws and convection-diffusion equations*, J. Comput. Phys., 160 (2000), pp. 241–282.

[15] L. C. G. ROGERS AND Z. SHI, *The value of an Asian option*, J. Appl. Prob., 32 (1995), pp. 1077-1088.

[16] H. G. ROOS, *Ten ways to generate the Il'in and related schemes*, J. Comput. Appl. Math., 53 (1994), pp. 43–59.

[17] R. U. SEYDEL, Tools for Computational Finance, Fifth ed., Springer-Verlag, 2012.

[18] S. WANG, *A novel fitted finite volume method for the Black-Scholes equation governing option pricing*, IMA J. Numer. Anal., 24 (2004), pp. 699–720.

[19] P. WILMOTT, J. DEWYNNE AND S. HOWISON, Option Pricing: Mathematical Models and Computation, Oxford Financial Press, 1994.

[20] H. WINDCLIFF, J. WANG, P. A. FORSYTH AND K. R. VETZAL, *Hedging with a correlated asset: solution of a nonlinear pricing PDE*, J. Comput. Appl. Math., 200 (2007), pp. 86–115.

[21] J. E. ZHANG, *A semi-analytical method for pricing and hedging continuously sampled arithmetic average rate options*, J. Comput. Finance, 5 (2001), pp. 59–79.